Dynamics of nanoscale droplets

Joel Koplik
Benjamin Levich Institute and Department of Physics, City College of the City University of New York, New York, New York 10031

Somnath Pal* and Jayanth R. Banavar
Department of Physics, The Pennsylvania State University, University Park, Pennsylvania 16802

(Received 23 January 2001; revised manuscript received 14 August 2001; published 16 January 2002)

Several aspects of the dynamical behavior of nanometer-sized liquid drops have been investigated using molecular dynamics computer simulations. The liquids consist of chains of lengths 2–100 with Lennard-Jones and nonlinear elastic interactions, comprising drops made of $O(100\,000)$ atoms with radius $O(10$ nm), placed on an atomistic substrate. We simulate the solidification of a liquid drop on a substrate as the latter is cooled, and observe a smooth contraction and smoothing process but no dimple formation. If instead we simulate heating of the substrate, the drop evaporates, and we find a decrease on contact angle in the partially wetting case, in accord with recent predictions. Last, we consider the coalescence of two such droplets, either spontaneously or when pushed together, to study shape evolution scaling laws and to document a rapid internal structural reequilibration. Aside from the intrinsic novelty associated with the small scale of these systems, the results illustrate the relation between atomic scale interactions and macroscopic continuum properties of materials.

DOI: 10.1103/PhysRevE.65.021504 PACS number(s): 61.46.+w, 44.35.+c, 47.55.Dz, 47.20.Dr

I. INTRODUCTION

This paper considers several aspects of the dynamics of nanometer-sized drops of liquid, based on molecular dynamics (MD) simulations [1]. Several considerations motivate these calculations. First, nanoscale devices for practical fluids applications are beginning to appear [2], and these can contain correspondingly sized bodies of liquid whose presence affects their behavior. Second, extensive recent experience [3] shows that the physics of many macroscopic processes can be correctly captured by nanoscale MD calculations, so the results are likely to have a more general relevance. Third, we will focus on a trio of specific calculations where the molecular information is either directly of interest, or else there is an issue of whether certain material assumptions at the continuum level are realizable in practice. Finally, the simulations presented here are illustrative of what can be achieved by MD methods in this context, and the techniques may be of more general applicability.

We study liquids made of chain molecules in contact with an atomic solid, in configurations corresponding to droplets placed on a substrate, and then study either their solidification as the substrate temperature is reduced, their evaporation as the substrate is heated, or else the coalescence of two such droplets placed in near proximity. We had originally anticipated some significant variation in behavior with the molecular size, and so we have considered molecular lengths of 2, 4, 10, and 100, usually (aside from one case) in the form of freely jointed chains. In fact, we observe the same qualitative behavior for all of these systems. In solidification we are motivated by suggestions in the literature concerning the solidified droplet shape: if a solid is only partially wet by its own melt, it is argued [4], and observed in one experiment, that when a sessile liquid drop solidifies by cooling of its substrate, a subdroplet or dimple will form on its top. In evaporation, the motivation is to consider contact line dynamics in the presence of heat transfer [5,6], and, in particular, to study the change in contact angle induced by substrate heating. In coalescence, we wish to extend earlier MD studies [7,8] for monatomic liquids, test a scaling law for the time dependent coalesced neck radius, and more generally to understand the subcontinuum stages of this process. The common feature of the three problems is that they begin from the same initial equilibrated configuration of a drop resting on a solid, and make use of essentially the same molecular models and computer code. The process opposite to coalescence, drop rupture, is both relevant and accessible to MD simulation, but these calculations will be the subject of a separate paper [10] that studies the extensional deformation of a liquid cylinder.

In Sec. II, we review the MD methods used here, and describe the protocol used to generate a drop in thermal equilibrium on a substrate. In essence, the liquid is heated into a disordered dilute state, which is then cooled and compressed to form a drop of disordered chain liquid. The liquid is placed on a substrate and allowed to reequilibrate before studying its response to changes in its environment. Section III discusses drop solidification, which is simulated in obvious imitation of laboratory experiment by just cooling the substrate. We study the evolution of the drop shape, as well as that of the internal density, temperature, and pressure fields. When the substrate is heated rather than cooled, we consider droplet evaporation in Sec. IV, based on the same initial configuration. Here, the focus is on the evolution of the liquid-vapor-solid contact angle. We then consider coalescence in Sec. V, simulated here by simply duplicating a drop plus substrate configuration, and moving one drop in space to be adjacent to the second. The drops are either allowed to coalesce freely, or else are forced together by substrate motion. Here, we are interested in the evolution of the

*Present address: Lawrence Berkeley National Laboratory, 1 Cyclotron Road, Berkeley, CA 94720.

coalesced shape, and the microstructural healing process as the combined system returns to equilibrium. Conclusions and avenues for further work are presented in Sec. VI.

II. INITIALIZATION

Our MD calculations are of a relatively standard form [1], and consider a fluid made of atoms interacting with two-body forces of two types, a Lennard-Jones (LJ) potential to provide an impenetrable atomic core and chemical attraction at larger distances, along with a finitely extensible nonlinear elastic (FENE) force to link the atoms into chain molecules. The explicit forms of the interaction potentials are

$$V_{\mathrm{LJ}}(r)=4\epsilon\left[\left(\frac{r}{\sigma}\right)^{-12}-\left(\frac{r}{\sigma}\right)^{-6}\right],$$

$$V_{\mathrm{FENE}}(r)=\frac{1}{2}kr_0^2\ln\left(1-\frac{r^2}{r_0^2}\right). \tag{1}$$

The Lennard-Jones interaction acts between any two atoms separated by a distance less than $r_c=2.5\sigma$, and the FENE potential [9] acts only between adjoining atoms in any one molecule. The parameters in the FENE potential are taken to be $r_0=1.5\sigma$ and $k=30\epsilon/\sigma^2$. The solid substrate upon which fluid droplets rest is an fcc lattice of atoms, which also have a Lennard-Jones interaction of the form above, except that an adjustable coefficient is used to modulate the strength of the r^{-6} attractive term between solid and liquid atoms to control the wettability (see below). The solid density is $0.60\sigma^{-3}$, and the lattice spacing is incommensurate with the minimum in the fluid potential. The integrity of the solid is maintained by tethering its atoms to fixed fcc lattice sites [11], using the harmonic spring potential $V_{\mathrm{solid}}=\frac{1}{2}fr^2$, with $f=100\epsilon/\sigma^2$. The solid atom mass is set to 100 times the fluid atomic mass, so that the the oscillation period about the potential minimum is roughly the same for solid and fluid, and a common time step may be used in integrating the equations of motion. The solid and fluid atoms are confined to a rectangular region of space either by periodic boundary conditions, in which case the minimum-image convention [1] is used for force evaluations, or else by soft walls, implemented with a repulsive r^{-12} potential.

A molecular liquid based on the FENE and LJ potentials (1) has been widely studied as an MD a model of polymer melts [12]. In most previous work, the 6–12 potential is cut off at a smaller value than used here, $r_c=2^{1/6}\sigma$, which has the computational advantage of reducing the number of atoms that are in interaction range, and speeding the calculation. The properties of this system are given in detail in Ref. [13]. This value of r_c corresponds to a purely repulsive potential which, while adequate for a confined material, has the disadvantage here that a fluid will expand to fill space uniformly, with no interface. Here, however, the interface is crucial, and we retain the larger r_c. The properties of our fluid have been measured in separate MD simulations, and are recorded in full in Ref. [10], but roughly speaking for chain lengths through 100 these are Newtonian liquids at the low strain rates relevant to this paper.

In order that these molecular results have some connection with larger-scale continuum processes, we adopt the rule of thumb that the drop should have a linear size at least 10 times the typical size of an individual molecule, leading to initial drops that are somewhat large by MD standards, $O(10^5)$ atoms. The calculations are, therefore, done in parallel on either a T3E, an Origin-2000, or an IBM SP, using a spatial domain decomposition algorithm and message-passing interface (MPI) routines [14]. Given the initial positions and velocities, the latter sampled from a Boltzmann distribution at the temperature of interest, the atomic positions evolve in time according to Newton's equations, integrated using the velocity Verlet algorithm with time step 0.005τ, where $\tau=\sqrt{\epsilon/m\sigma^2}$ and m is the atomic mass. (The Verlet algorithm for differential equations is advantageous for parallel computations because it involves only positions and velocities, so that it minimizes the amount of data storage and interprocessor transfer.) The substrate temperature is maintained at its prescribed value at all times, and the fluid temperature during the preparation stages only, using constant kinetic energy rescaling. More physical methods are available, but since the thermostatting is applied to the liquid only during the initialization stage, the simplest procedure suffices. Further discussion of MD calculations along these lines may be found in Ref. [3].

In the remainder of this paper, and, in particular, in all figures, when dimensions are not given we are implicitly using ''MD units'' where σ is the unit of length, τ is the unit of time, and ϵ the unit of energy. Typical numerical values might be $\sigma\sim 3$ Å, $\tau\sim 1$ ps, and $\epsilon\sim 100k_B$.

The liquid atoms are placed initially in a spatial arrangement convenient for book keeping, with 125 500 atoms grouped into chains of length 100, and 108 000 atoms in chains of length 10, or 32 000 atoms in dimer molecules, occupying adjoining sites on a fcc lattice of density 0.8 filling half the volume of a cube. The walls are impermeable, based on the repulsive potential described above. In the first stage of the calculation the positions are randomized by ''cooking'': the system is run at a relatively high temperature (3.0) and low density (0.4) until the time-averaged spatial density of atoms is uniform, the probability distribution of molecular sizes reaches a steady state, and the probability distribution of molecular orientations is rotationally invariant. The measure of molecular size used here is the radius of gyration, and the orientational measures are the angles between a molecule's end-to-end vector and two of the coordinate axes. (More refined measures of orientation may be defined using the eigenvectors of a molecule's inertia tensor, but for our purposes there is little qualitative difference [15].)

Once the high temperature fluid reaches a statistically stable disordered state, the temperature is gradually lowered to a value in the liquid-gas coexistence region for the density at hand (1.0 or 1.5, for lengths up to 10 and 100, respectively). At the same time, a weak central force is applied to each atom, $\mathbf{F}_i=-k_c(\mathbf{r}_i-\mathbf{r}_c)$, where $k_c=0.1$ and $\mathbf{r}_c$ the box center, to force the fluid to condense into a single spherical drop in the middle of the box. Once the squeezed drop reaches a stable radius, the central force is gradually released, and the liquid relaxes to an equilibrated spherical drop. In general, there can be vapor present as well, which is

evident for smaller chain lengths, but the longer chain systems tend to have so little volatility that it is rare to see a vapor molecule in simulations at this temperature and drop size.

The final stage of ''sample preparation'' is to generate a suitable liquid drop sitting on a solid surface. We take slightly more than the upper half of the spherical drop generated as described above, and rigidly translate all of the atoms therein to new positions such that a near hemisphere of liquid sits just above a solid substrate. The remaining liquid atoms that constituted the lower part of the drop are eliminated from the calculation; more precisely, we completely delete any molecule in the drop, which contains an atom below a reference plane just below the sphere center. The resulting semidrops contain 70 000, 58 520, and 16 232 atoms, respectively, for chain lengths 100, 10, and 2. The solid substrate consists of a layer of fcc cells containing 16 384 solid atoms in a square of side 100σ, which has been equilibrated separately from the liquid, which is then exposed to the 111 face. This system is allowed to reequilibrate at the same temperature before beginning one of the numerical experiments below. During this stage, the drop comes closer to the solid as the molecules near the bottom are attracted to those of the solid, and the shape of the drop adjusts to give the appropriate contact angle and spherical-cap shape. The reequilibration continues until the drop shape and local density field stabilize, a duration of 1000 and 150τ for chain lengths 10, 100, and 2, respectively. In the solid-liquid Lennard-Jones interaction, the coefficient of the r^{-6} term is reduced from 1 to 0.8, which in previous drop simulations [16] gave partially wetting liquids, and, indeed, we see stable, static drops with this choice of interaction.

III. SOLIDIFICATION

Our first application concerns the final *shape* of a droplet of liquid that solidifies when placed on a cold substrate. Specifically, we wish to test the suggestion of Anderson, Worster, and Davis [4] concerning the solidification dynamics of sessile liquid drops that solidify upwards from their base as heat escapes downward through the substrate. These authors argue that when the material has the property that its solid phase is only partially wetted by its own melt, such a droplet will solidify with a dimple on top. These authors present quantitative arguments for the suggestion, based on examination of the contact angle statics and dynamics of the system, but the idea can be understood by considering the intermediate stages where the drop has solidified only up to a certain height with a spherical cap of liquid remaining on top. If, in fact, the liquid only partially wets its own solid, one expects a change in slope at the transition height because the solid-melt contact angle required by capillarity (balancing of the various surface tension forces) need not agree with the slope that the solidified region has developed at that point (the result of heat and mass transfer and compressibility considerations). In fact, if the drop were to remain a spherical cap, the latter slope would decrease smoothly to zero approaching the top, so the mismatch in slope can grow as the solidification front moves upwards, and eventually there would be a small liquid drop sitting atop a solidified base, which could be small enough to solidify *in situ* before it can adjust its shape any further.

In this scenario, the principal uncertainty is whether any real liquid has the property that it does not wet its own solid. A related and well-known material property is that of autophobicity [17], the inability of certain fluids to spread on their own absorbed films on certain substrates. The origin of this behavior is the loss of configurational entropy due to the restrictions on the molecular configurations resulting from pinning of molecules by the solid, and is observed, for example, for polar liquids on high energy surfaces and for end-grafted polymers. In the case of solidification there is no obvious counterpart to this pinning mechanism, however. The original paper [4] gives experimental verification using a water drop on an aluminum substrate. Now large-scale MD simulations of water are difficult because a long-ranged Coulomb potential is involved, which leads to computation times varying as the square of the number of atoms present. Feasible MD calculations with Coulombic forces typically involve only $O(10^3)$ atoms, and in such small drops it is difficult to distinguish atomic scale fluctuations from ''bulk'' shape changes. The short-ranged potentials used here apply to uncharged but polarizable molecules, which are sometimes used to mimic water by varying the coefficients. In the absence of any outside guidance, we have resorted to trial and error, and performed solidification simulations with a variety of different liquids. One of the advantages of MD simulations, and a reason for addressing the question in this way, is that we are able to vary the microscopic structure in a controlled way to see if and how the solidification dynamics differ. In contrast in a continuum calculation the required wetting properties would be (mathematically) assumed. A second motivation is that the argument for dimples, at least as presented above, suggest that they could be small and difficult to observe in an experiment, whereas these simulations resolve individual atoms.

Aside from examining the droplet shape, we can also study other relevant quantities such as the internal temperature and density fields, and the individual or averaged atomic displacements under cooling. There is some relevance in doing so for nanometer-sized droplets, since there are questions about how well such systems are described by bulk thermodynamics. It is known, for example, that for droplets in the 100-atoms size range there is a finite range of temperatures where liquid and solid coexist, rather than the single temperature found in the thermodynamic limit [18]. A further question is whether different (simple) molecular models give different behavior; we have considered homogeneous systems made of freely jointed chain molecules of lengths 2, 10, and 100, and a 50-50 mixture of chains of lengths 2 and 4. We also considered a nematiclike liquid made of semirigid chains of length 4, with an additional bond-bending interaction $V_{BB}=(1/2)k_{BB}\cos(\theta-\theta_0)^2$, where θ is the angle between adjacent ''bonds'' in a molecule (the vectors joining the centers of adjacent atoms), and θ_0 the preferred value.

Our results are that for all systems tested, a liquid drop solidifies into a spherical cap, with no dimple. It is possible that we simply failed to examine the right material, but at

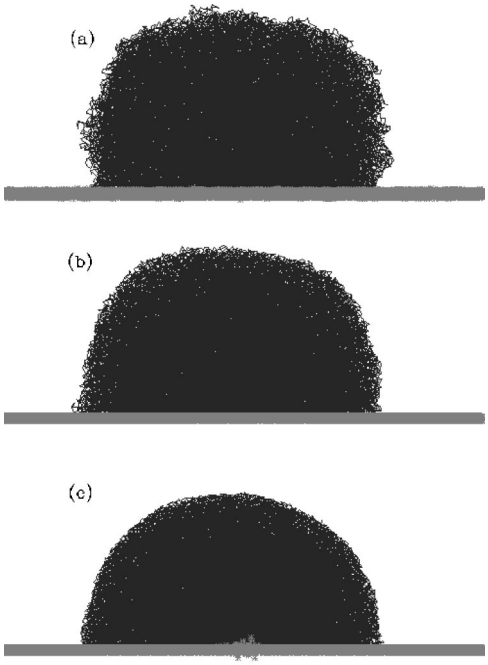

FIG. 1. Snapshots of a solidifying drop of length-100 chains molecules at times (a) 0, (b) 1500, and (c) 6000τ.

least within the spectrum covered there is nothing unusual about shapes in solidification. In fact even the quantitative results have essentially the same features, so we focus on one case—chains of length 100. The cooling protocol is that after the equilibration described above, the substrate temperature was set to a fixed low value (0.1 for chain lengths up to 10 and 0.15 for length 100, one-tenth of the respective liquid values during equilibration) and the liquid was allowed to evolve freely. Figure 1 shows the drop just before cooling begins, at an intermediate stage, and in the final state of the simulation at an average temperature 0.21: the boundary smoothens while the entire drop contracts, and no dimple forms. These figures are three-dimensional views of all of the atoms in the simulation, as seen from a long distance. The substrate atoms are shown as + signs, and the molecules are represented as the set of straight line segments joining the successive molecules in each chain. Because of the large number of lines and the finite resolution in the figure, the bulk of the drop appears as a smoothly filled region, aside from a few small gaps. Although the interior positions of the atoms are poorly resolved in this plotting format, the outer boundary of the drop and the shape evolution are quite clear.

In this case of chain molecules the solidified structure is amorphous, but in Fig. 2, we show a contrasting example with local crystalline order in a different material—a dimer molecule system, at time 3500τ, when the average temperature has dropped to 0.281. In this case the molecules are small enough to settle into position in register with the substrate lattice, whereas the longer molecules are unable to do so. The latter amorphous solidification behavior is seen in the other examples we have studied, length-10 chains and length-4 nematics. Returning to the length-100 chains, the time decay of the average temperature is given in Fig. 3(a), roughly an exponential decay after a transient (more precisely, a superposition of exponentials is expected). The average pressure and density within the drop rise as temperature falls, and these quantities are plotted in Figs. 3(b) and 3(c), respectively. The pressure is obtained from the standard virial expression [1], with the boundary regions excluded as described in the next paragraph. Again, the other molecular systems show the same qualitative behavior.

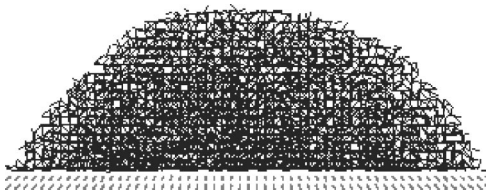

FIG. 2. Snapshot of a solidified drop of dimer molecules at time 3500τ and temperature 0.281.

To obtain the local fields, the system box is first divided into slabs of equal thickness (1σ), and at each time step and within each slab, the drop's center of mass is located and used as an origin of polar coordinates. Concentric disks of equal radial spacing are used as sampling bins to accumulate density, temperature, and stress, etc. An average of the binned quantities is taken at 50τ intervals, and stored. Fully three-dimensional binning is possible, but previous experience indicates that in this case the samples are too small and the results too (statistically) noisy to be useful [19]. When the binned data is examined directly, we observe a rapid variation near the edge of the drop, and otherwise density is constant while stress, temperature and mean-square displacement vary systematically with height (y). A temperature example at time 1500 is given in Fig. 4. Although the constant-T contours meander a bit, the most significant variation is with height, so we average over the other directions, retaining those bins where the density exceeds a lower cutoff of 0.1. (The thick lines at the edges of the drop in this figure reflect the fact that the temperature changes rapidly there to a zero value outside the drop.) The resulting local temperature field within the drop is approximately a function only of height off the substrate, and is shown at successive times in Fig. 5(a). As an alternative to temperature, we also considered the variation of the average atomic displacements with time, evaluated by the same method as for temperature. To be precise, we measure the mean-square atomic displacement over a 50τ time interval for atoms in a slab of thickness σ centered at a particular value of y, $\langle R^2(y)\rangle$. This quantity, shown in Fig. 5(b), behaves similarly to the temperature—a weak variation with height at any fixed time, with substantial fluctuations near the edge of the drop where the molecules are unconstrained on one side, and a gradual decay with time and global temperature. Note, in particular, that at late times, the typical atomic displacements are negligibly small, which allows us to conclude that the material has solidified.

Note that the value of y at which each curve terminates decreases systematically for times up to about 3500τ, as the drop contracts under cooling, but that there is no significant height variation at later times. Similarly, the mean-square displacements are quite small after this time. One might then say that the drop has ''solidified'' at this point, at temperature

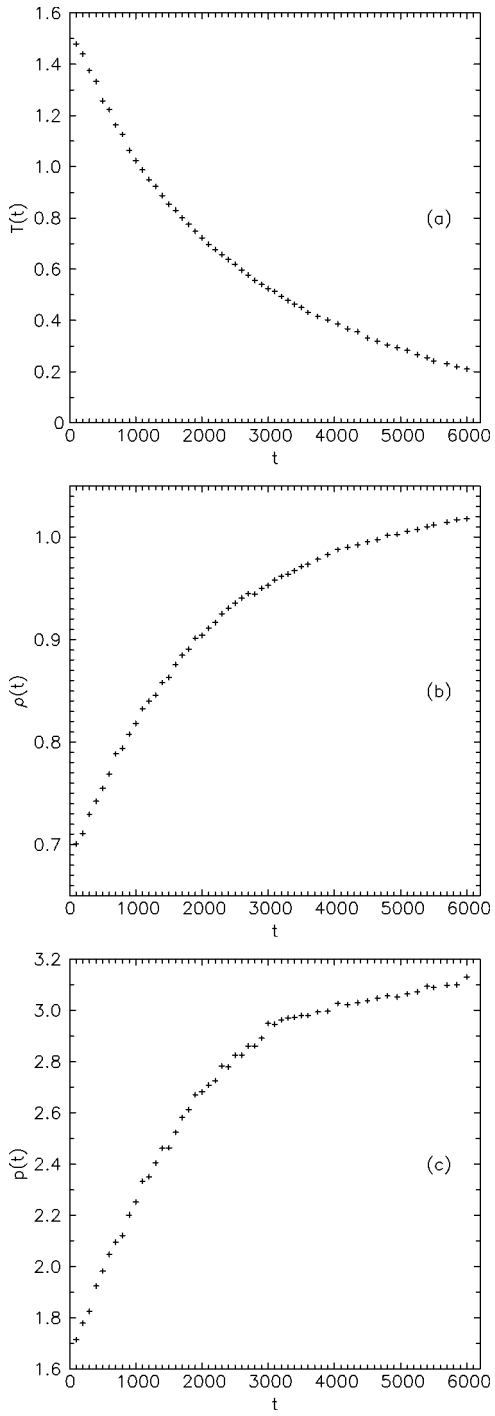

FIG. 3. Time variation of the average values of (a) temperature, (b) density, and (c) pressure, for the solidifying drop of length-100 chains shown in Fig. 1.

around 0.49. In calculations of solidification in a variant molecular model with the Lennard-Jones interaction is cut off at $2^{1/6}$ [20], a more liquidlike behavior is observed at this temperature, but the absence of the attractive potential tail permits more freedom in the atomic motion, other thing being equal, and one would expect a lower freezing temperature in that case.

The molecular structure, as measured by geometrical quantities such as the distribution of radii of gyration or molecular orientation angles, shows no interesting systematic variation either with height off the substrate or with time. The one exception to this statement is the tendency of molecules close to the substrate to orient parallel to it, an obvious packing effect. Presumably the drop solidifies on a time scale short compared to that required for molecular rearrangements, and the initial uniformity of the molecular orientations is preserved in the bulk. A question we are not able to explore easily is the effect of cooling rate: the substrate temperature is already quite low, and still smaller values would not likely make any significant difference, but it is possible that the behavior of solidifying drops would differ at much lower cooling rates, (corresponding to extremely lengthy MD simulations) where there is more time for the internal structure of the liquid to vary. Likewise, in this vein, it is conceivable that dimple formation is a very slow process on molecular time scales, whereas our simulations used a relatively rapid cooling protocol that could conceivably have frozen the molecules in place before a dimple could evolve. We regard this explanation as unlikely, since previous MD simulations of wetting phenomena on time scales similar to those studied here do not observe such clear shape discrepancies, but cannot rule it out.

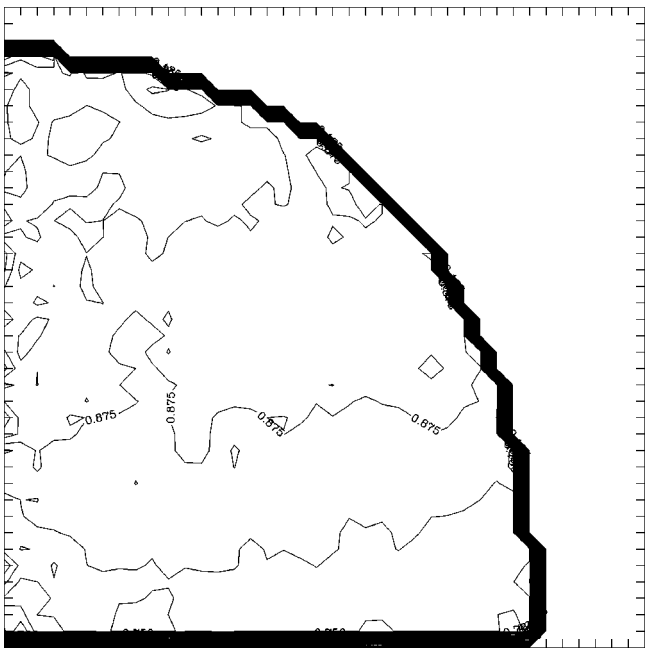

FIG. 4. Temperature field in a solidifying drop of length-100 chains at time 1500τ. The horizontal and vertical axes are radius and height, respectively, and the curves are contours of constant temperature, at intervals of 0.025. The heavy lines represent the drop boundary, where there is a rapid temperature variation. The outer boundary appears jagged rather than smooth, because in obtaining this figure low density regions are arbitrarily set to $T=0$.

IV. EVAPORATION

It is just as easy a simulation to heat the solid to study evaporation as it is to cool it for solidification. Specific motivation arises from recent studies of contact line dynamics in the presence of heat flow, in one case focused on a hot drop-

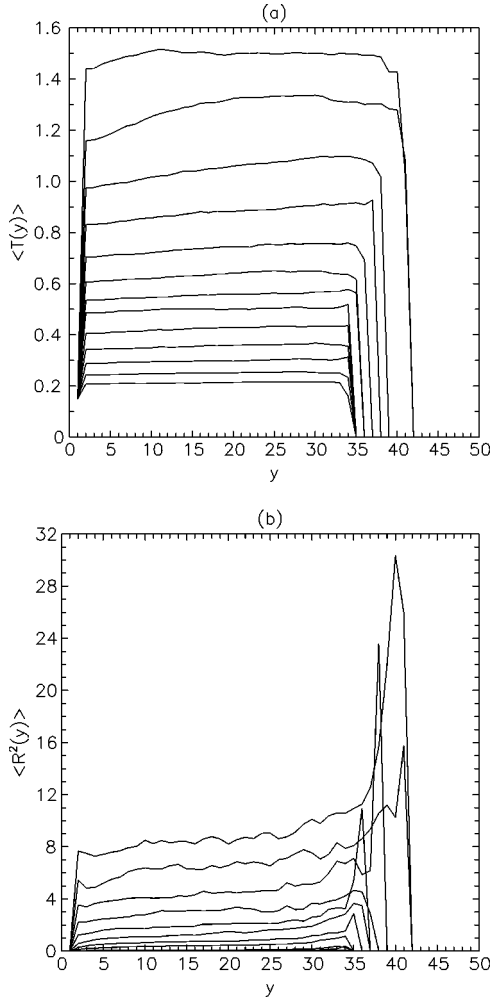

FIG. 5. Relaxation profiles in a solidifying drop of length-100 chains at times 0, 500, 1000, . . . ,6000τ (top to bottom): (a) temperature, and (b) mean-square atomic displacement, as a function of height *y* above the substrate. The temperature and displacement are set to zero where the density falls below 0.1, so the figure also indicates the contraction of the drop upon cooling.

let that spreads on a cooled substrate and so simultaneously tries to solidify and expand [6], and secondly a prediction for the change in contact angle as a thin droplet evaporates [5]. The spreading problem requires a sophisticated analysis, since one expects that there will be regions exhibiting clear solidlike and fluidlike behaviors, plus (at the molecular scale at least) a transition zone of ''mushy'' material. Furthermore, in the most obvious modeling, one has to deal with contact line singularities in both the shear stress and the heat flux. In the second problem, it is argued that under evaporation the contact angle will *decrease*, a somewhat counterintuitive behavior as one might argue naively that the thinner regions at the edge of the drop will heat up first and evaporate more rapidly, producing instead a larger contact angle. Here we focus on this simpler case, since it is straightforward to identify variations in contact angle, and leave the more difficult spreading problems for future work.

We consider one of the same initial drops as above, containing 58 520 atoms in length-10 chains, initially with both

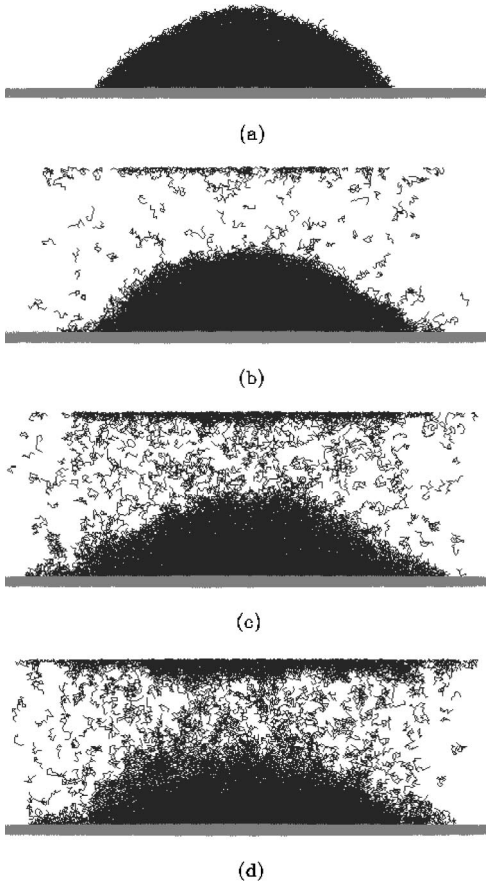

FIG. 6. Snapshots of a partially-wetting evaporating droplet at times (a) 0 (after equilibration, just before the substrate is heated), (b) 2500, (c) 5500, and (d) 8500τ.

drop and substrate at $T=1.2$, but with the solid-liquid interaction strength increased to 0.95. The reason for the latter modification is that the analysis motivating this calculation in Ref. [5] assumes a small contact angle, to justify use of the lubrication approximation. Here, however, a drop with a small contact angle in a system of modest size has much of its mass contained in a broad submacroscopic edge of only a few molecules thickness, which evaporates immediately. We assume that the key feature is partial as opposed to complete wettability, and compromise on a finite initial contact angle of about 45°, that require an enhanced solid-liquid interaction strength above the previous value 0.8 that gave a contact angle close to 90°. After 500τ of further equilibration after resetting the temperature and interactions, the previous drop spreads slightly and then stops, with the overall shape and shown in Fig. 6(a) (in the same format as the previous section). The substrate temperature is then abruptly raised to 2.0, while a second cold solid boundary at the top of the simulation region collects the evaporated molecules by condensation.

The simulation proceeds as shown in the remainder of Fig. 6. Initially the system has little vapor, but as the drop heats up, more and more is produced, to the point where the distinction between liquid and vapor is obscured. The visualization format used in Fig. 6 is awkward in this context since the three-dimensional information on atomic positions

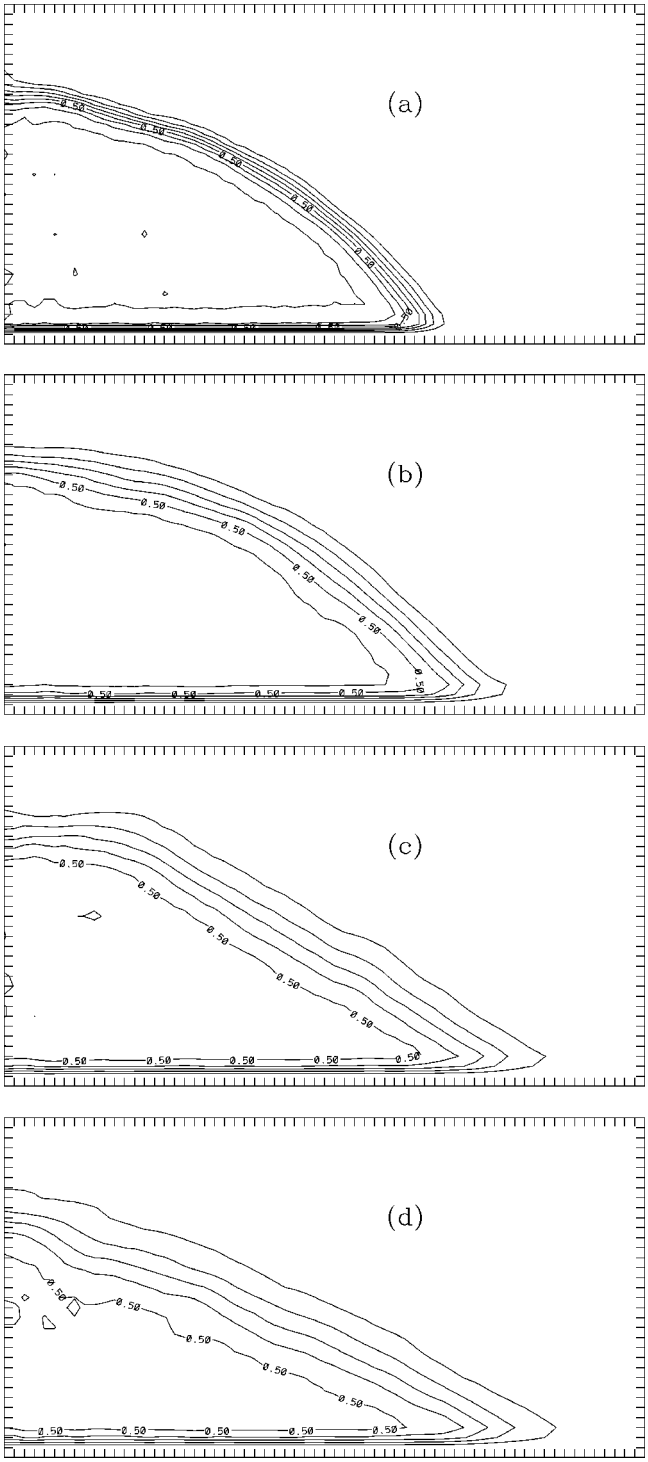

FIG. 7. Contour plots of fluid density during evaporation, in one-to-one correspondence with the snapshots in Fig. 6. The density 0.5 contour is so labeled, and the others are at intervals of $0.1\sigma^{-3}$; the tick marks on the axes are spaced by 1σ.

is unclear, but liquid and solid may be clearly distinguished in the density contours of Fig. 7. To obtain the latter figures, the atomic positions are cylindrically binned and averaged over a 25τ time interval, and lines of constant density as a function of the radial and vertical coordinates are plotted, with regions of density below 0.1 ignored. The contact angle is identified as that made by the group of parallel contours at the edge of the drop with the horizontal, and we see that the value decreases to about 30°, just the trend predicted by [5]. Eventually, the drop is reduced to a thin pancake and evaporates completely to form a uniform fluid phase in the simulation region, but there is an interval of about 5000τ (roughly from times 3500 to 8500) where the contact angle stabilizes at the reduced value. Another notable feature of the density contours is the thickening of the interfacial region where the density drops from its central value to the nominal edge value 0.1. This thickening is present but much reduced on the base of the drop, which remains in close contact with the heated substrate in this case.

Further time-dependent characterization of the drop behavior is given in Fig. 8. We (arbitrarily) define the liquid drop as the region where the density exceeds 0.1, and average over it. The average temperature [8(a)] rises to the substrate value and fluctuates around it slightly, while the internal temperature field is similar to that in the solidification case, approximately constant within the drop, aside from a weak decrease in the vertical direction. The average density in the drop [8(b)] decreases systematically with time, while the average pressure [8(c)] drops initially and then fluctuates about a reduced value. The height of the drop fluctuates about the unheated value roughly until time 2000, and then decreases as the drop forms a pancake and evaporates completely.

We have also simulated the heating of two other systems: in a liquid made of length-100 chains, we see similar results—a decrease of contact angle accompanying the evaporation, while in the case of dimer molecules, the system becomes so volatile on heating that it is difficult to identify a contact angle at all. Although we are not in the parameter range for a detailed quantitative comparison, the trend observed here of *decrease* of contact angle on heating supports the analytic arguments in Ref. [5].

V. COALESCENCE

The coalescence of liquid interfaces is a ubiquitous process in nature, whose microscopic aspects are infrequently studied. There is extensive recent work on the continuum asymptotics of the reverse process, interface rupture [21], which has been extended, in part, to study the dynamics of two drops that have recently contacted each other, and which have merged over distances ''large'' compared to molecular sizes [22]. Here, the size of the merger region must begin at lengths large enough for a continuum analysis to apply, and extend far enough outwards for scaling arguments to be applicable. The only calculations that consider the merger process itself are two MD studies of drops of monatomic Lennard-Jones liquid, a rather volatile material with substantial coexisting vapor in equilibrium, and a very diffuse liquid-vapor interface. In one case [7], the interface was sharpened by placing the drops in an immiscible background fluid, and the drops were made to coalesce by subjecting the background fluid to a shear flow. (Without flow, coalescence is prevented by lubrication forces arising from the background liquid film between the drops.) A second monatomic

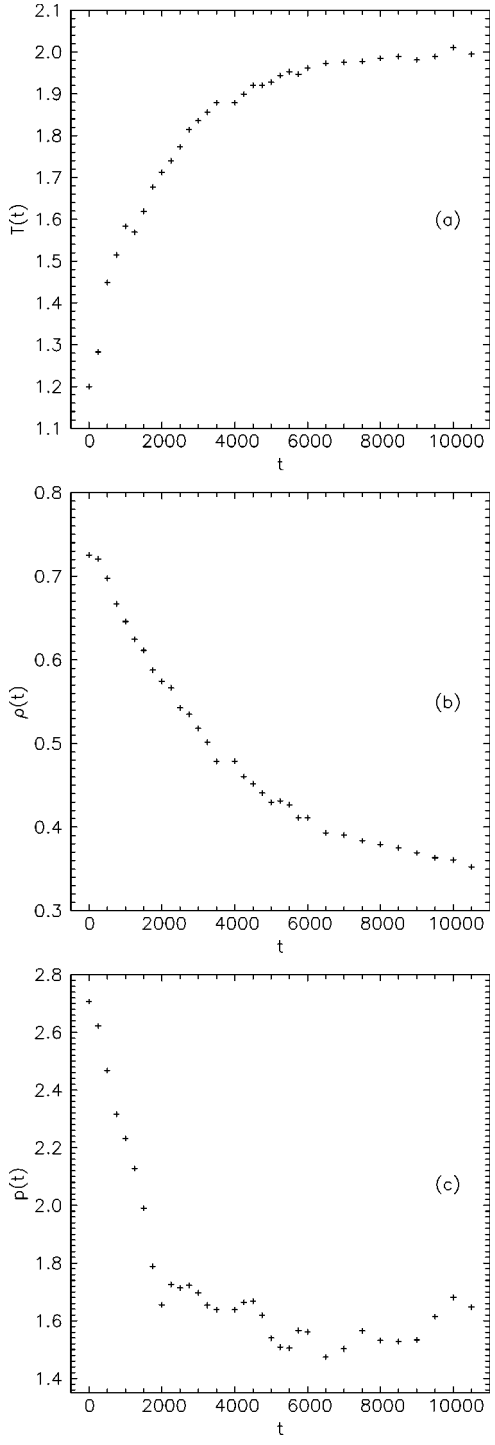

FIG. 8. Time dependence of (a) average temperature, (b) average density, and (c) average pressure. The substrate and drop are equilibrated at $T=1.2$ for 300τ, whereupon the substrate temperature is raised to 2.0. The criterion distinguishing the (liquid) region from its vapor is a density cutoff of $0.1\sigma^{-3}$.

drop calculation considered a drop placed near a bath of the same liquid, with only vapor present [8]. This case addressed a different issue, whether relative motion would suppress coalescence, and the fact that vapor obscured the fine structure of the coalescence process was not relevant. Here, we wish to consider coalescence of drops of a single liquid with little or no vapor and no extraneous background material present. Both free and forced coalescence are considered, using molecular liquid in the form of FENE chains of various lengths. Aside from investigating the molecular motion associated with coalescence, we study the ''healing'' of the merged liquid—the return of its internal structure in the junction region to its original state.

We will present a detailed discussion and results for one case, chain molecules of length 10, and then compare the behavior of other lengths. We begin with a previous configuration of a partially wetting drop on a substrate, with 58 250 fluid atoms at temperature 1.0, and replicate both drop and substrate to give the configuration shown in Fig. 9(a). The replication procedure consists of taking a copy of the original system (i.e., the set of atomic positions and velocities), and modifying the velocities by adding a uniformly distributed random number in the interval $[-v_{th}/2,+v_{th}/2]$ to each component of each fluid atom's velocity. (Here, $u_{th} \equiv \sqrt{k_B T/m}$ is the thermal velocity in each spatial direction). The replicated system is then evolved in time, with a thermostat applied, until it returns to equilibrium, as evidenced by a Boltzmann velocity distribution and a stable drop shape. It is then translated and flipped over ($z_i \rightarrow z_{max} - z_i$ and $v_{zi} \rightarrow -v_{zi}$ for all atoms i), with the new position of the replicate chosen so that its atoms are just within range of the potential of the first drop, a minimum atomic separation of 2σ, and for free coalescence the two-drop system is simply allowed to evolve. For forced coalescence at relative velocity v_0, motion of the substrates is used to drive the drops together. In this case all atomic z velocities in the upper/lower drop are initially shifted by $\mp v_0/2$, and the drops are allowed to evolve while the substrate tether positions continue to move at these velocities.

A sequence of snapshots of the two-drop system is shown in Fig. 9, indicating a smooth final shape by time 2000τ, in the nanosecond range. The figure is a three-dimensional view of all atoms in the liquid, viewed from a distance, in essentially the same format at Fig. 1. In this case, all molecules originally in the lower drop are plotted first, then those originating from the upper drop are drawn at a darker gray level, and superposed on the previous ones if necessary. The resulting figure gives first the outline of the entire drop, and second the part of the drop occupied by the upper fluid as the darker region. We see a significant amount of interpenetration of the two original drop molecules, and this mixing can be quantified by giving the separate density profiles of the atoms of the two drops as a function of vertical position (y). The result, Fig. 10, indicates a rather generic quasi-one-dimensional mixing process: reading from left to right in Fig. 10(a) at time 250, for example, the curve initially follows the hemispherical outer boundary of the lower drop, then intersects the upper drop at $y \approx 33$, whereupon it steepens in the central mixing region, and finally decays smoothly to zero. At the later time 1000τ in Fig. 10(b), the outer boundary of the merged two-drop system is closer to conical (cf., Fig. 9), while the mixing region has broadened. Aside from the outer drop boundaries, each profile resembles the standard error function solution of the diffusion equation. The more surprising feature is relaxation of the merger region to the pre-

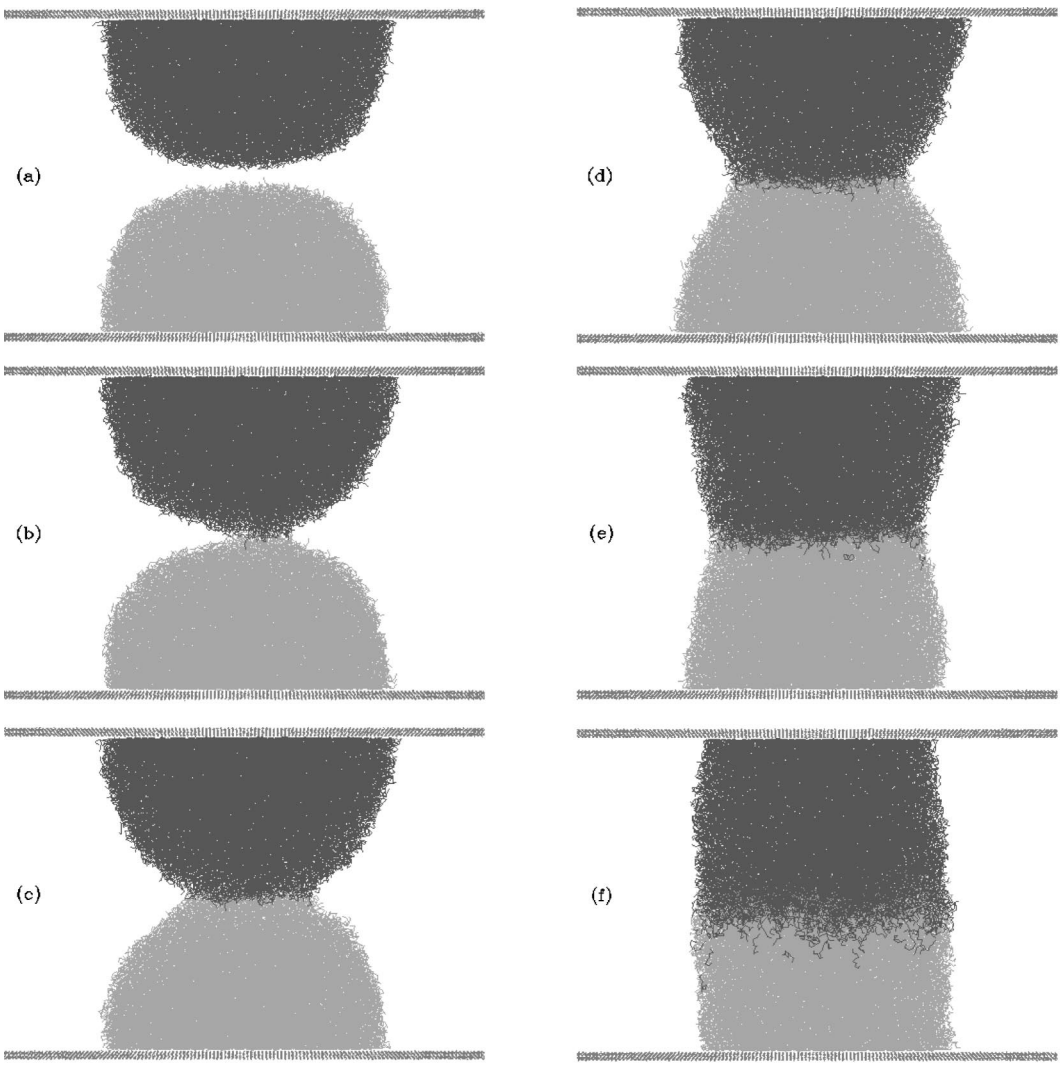

FIG. 9. Coalescence of two liquid drops of length-10 molecules at times (a) 50, (b) 100, (c) 150, (d) 250, (e) 500, and (f) 2000τ. Molecular positions in the upper drop are overlaid on those in the lower drop, to indicate the degree of mixing.

merger behavior. Figure 11 shows the profiles of total density and mean-square displacement (over a 50τ interval). The density has an initial dip in the center, associated with the gap between the original drops, which fills in after 200τ to give a uniform profile roughly at the same value as before merger. The displacements are initially unusually large in the central region, because the atoms there are free to move into the gap, and this peak grows to a maximum as molecules are drawn from one drop to another. Again, by time 300τ, the peak is gone and the displacements are uniform across the merged-drop system.

With regard to the shape of the merged-drop system, note that the contact angle the liquid makes with the solid has not quite reached the value before merger, indicating that the liquid has not yet reached hydrostatic equilibrium. Note also that the four contact angles visible in the premerger snapshot are slightly different, a small-system statistical fluctuation property often observed in MD simulations. Snapshots at intermediate times not displayed here likewise show that the boundary of the merged liquid is still moving at time 2000. In fact, one would normally expect some sloshing motion subsequent to drop merger, so this behavior is expected.

In Ref. [22], continuum arguments are presented that the (minimum) radius of the neck of the coalescing two-drop system would vary with time as $r_m \sim t \ln t$, and that the width of the gap would vary as r_m^3. To test these results, we determine the neck radius by examining density contours, and using the minimum radius of the contour corresponding to half the bulk density. The time variation of neck radius is shown in Fig. 12, for homogeneous liquids of chain lengths 2, 10, and 100. The length-2 chains merge very rapidly compared to the other cases, partly because the initial drops were smaller by a factor of about 2, and also because this liquid is quite volatile while the longer chains are not. In all cases the behavior of the neck radius does not agree with theory. One reason for disagreement is that the neck is perhaps not yet thick enough to be described by the Navier-Stokes equations at short times. A second source of discrepancy is that the drops are quite small and at later times the neck size is not far from the drop size, so that the later behavior is affected by volume conservation constraints, whereas the analysis in Ref. [22] assumes that the original drops are large enough to

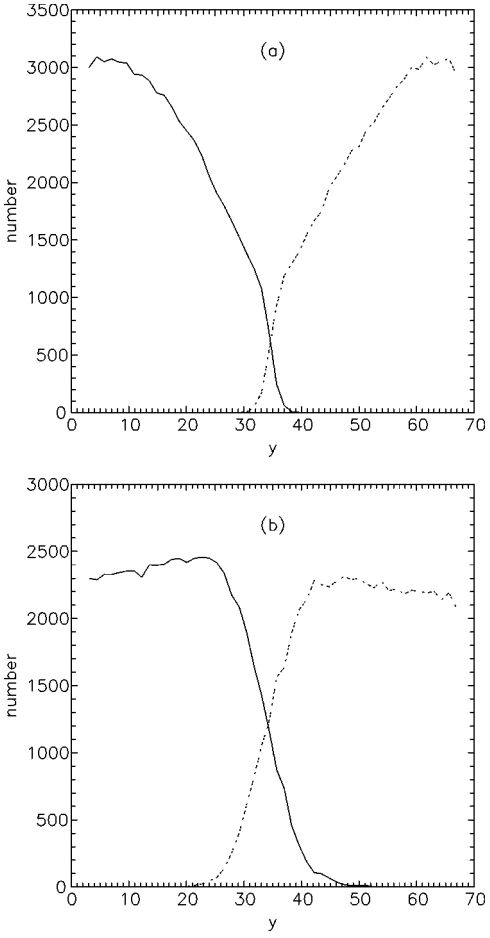

FIG. 10. Number of atoms of each (original) drop as a function of height in Fig. 7 at times (a) 250 and (b) 1000τ.

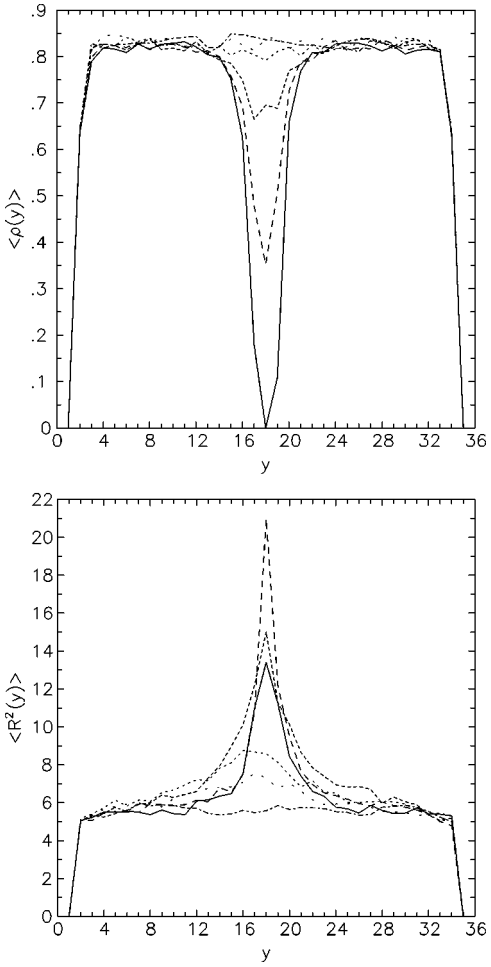

FIG. 11. Profile of (a) atomic density and (b) mean-square displacement as a function of height for the coalescence sequence in Fig. 7. The different curves refer to times 50 (—), 100 (– –), 150 (- -), 200 (· ·), 250 (· ·), and 300τ (– · –).

become spherical away from the coalescence region. A third difficulty is that, remarkably, the two polymeric liquids merge at essentially the same rate despite having different properties, including a viscosity ratio of 2. This observation suggests that the merger process here is not dominated by viscosity. The width of the gap is not straightforward to compare with theory, since it is defined as the width where the high curvature merger region matches onto asymptotically straight sections, and it is difficult to identify such a location in the results here. If we use the distance between the upper and lower points of inflection of the same half-bulk-density contour as above, we find that the gap increases with time, but do not observe any simple power law behavior.

In Fig. 13, we zoom in on the gap region between the drops during the initial stages of coalescence, showing the interpenetration of the individual molecules. We see a merger mechanism similar to that found for monatomic liquids in Ref. [7]: atoms in molecules near the surface occasionally fluctuate out of the drop and eventually atoms from the two respective drops fluctuate to within interaction range and attract each other. As they move together they draw their respective molecules along with themselves, and these, in turn, draw their neighboring molecules outward. The process cascades as more and more molecules of one drop are drawn towards the other, and a tendril of liquid forms joining the

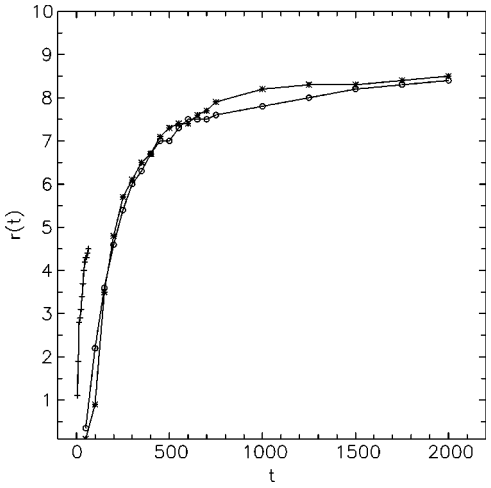

FIG. 12. Neck radius of coalescing drops as a function of time for chain lengths (+) 2, (×) 10, and (o) 100.

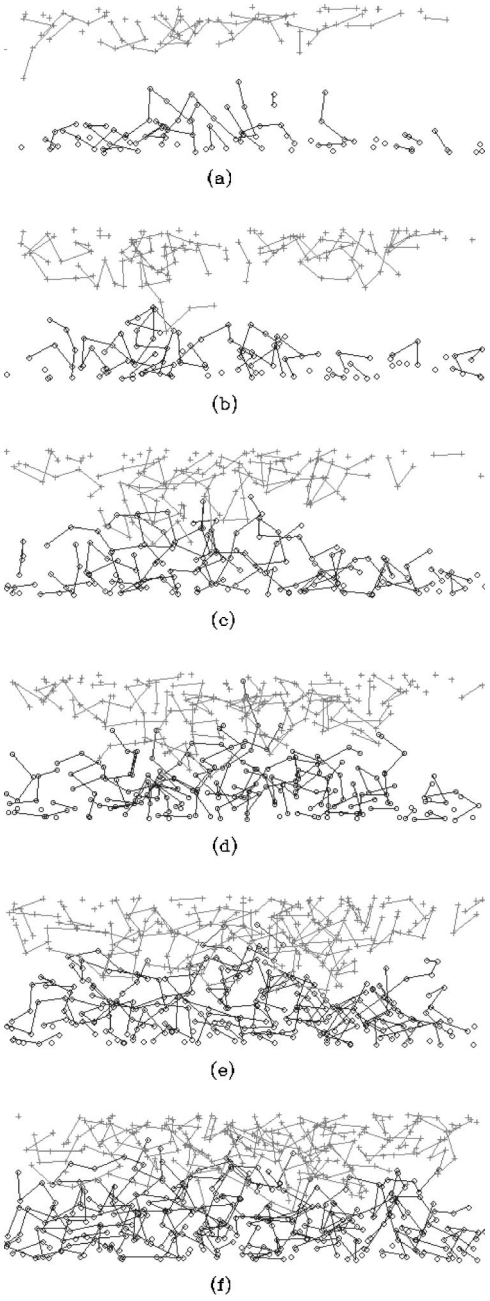

FIG. 13. Snapshots of the merger region of two coalescing length-10 droplets, shown in full in Fig. 7, at times (a) 70, (b) 75, (c) 80, (d) 85, (e) 90, and (f) 95τ. In each frame, only those atoms occupying a slab in the merger region of thickness 5σ are shown, those in the upper drop as $(\times)$, and those in the lower drop as (o), and if two adjacent atoms in the same molecule are in this region, the bond between their centers is shown as well.

two drops, and as the tendril thickens the drops merge.

The previous plots show that as far as single-atom motion is concerned, the merger region heals after coalescence within sub-nanosecond time intervals. A more subtle test of atomic equilibration is the spatial correlation between pairs of atoms, and to analyze this question we have computed the pair distribution function [26] at various points. We consider all atoms within a test sphere of radius 10σ and compute the

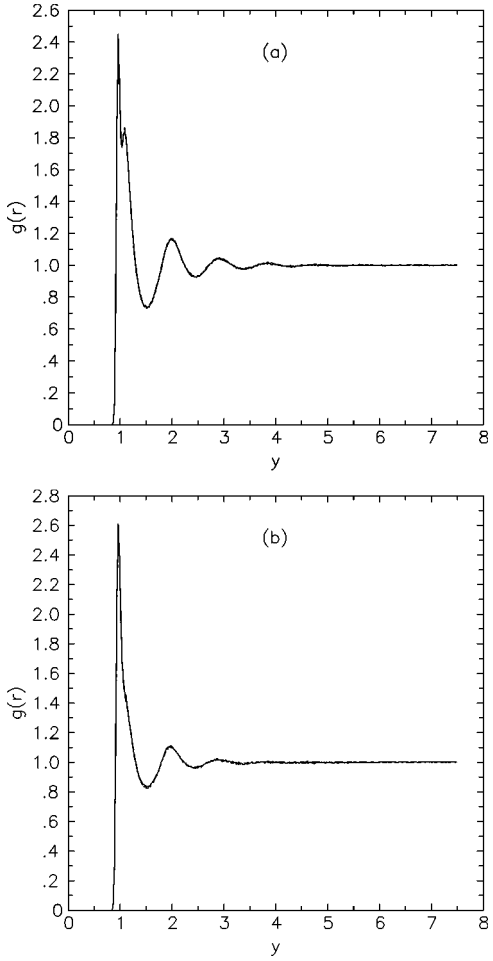

FIG. 14. Radial distribution functions in coalesced drops: (a) length-10 chains and (b) length-100 chains. As discussed in the text, each plot contains four separate curves taken at different times and locations, which show no significant variation.

probability that a second atom is at a given separation r, averaged over a 25τ time interval. The result for length-10 chains is shown in Fig. 14(a), where we actually superpose four different cases—test spheres in the lower bulk liquid and in the coalescence region, each at times 300 and 2000τ. The curve shows a split nearest neighbor and clear first, second, and third next-nearest-neighbor peaks, as would be expected in a condensed liquid. The same result, up to minor statistical fluctuations, is obtained in the original spherical free-floating drop as well, and represents the equilibrium pair distribution. There is no significant variation in these distributions, and as far as two-atoms correlations are concerned, the system has healed by time 300τ. If we consider length-100 molecular chains, the result in Fig. 14(b) shows less structure in that only two secondary peaks are evident, but again there is no significant variation with time or spatial region with the two-drop system.

We have also considered further structural measurements of the internal configurations—the molecular radius of gyration and orientation, the latter defined as the angle between a molecule's end-to-end vector and the vertical axis normal to the substrate joining the drop centers. Sorting the molecules

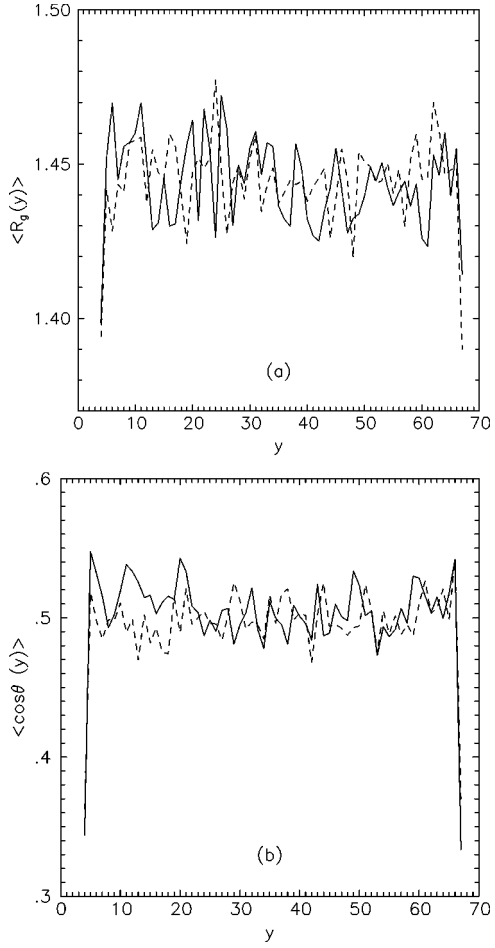

FIG. 15. Molecular relaxation after coalescence of length-10 chains as a function of height: (a) radius of gyration and (b) cosine of the orientation angle. The solid and dashed curves refer to times 300 and 2000τ, respectively.

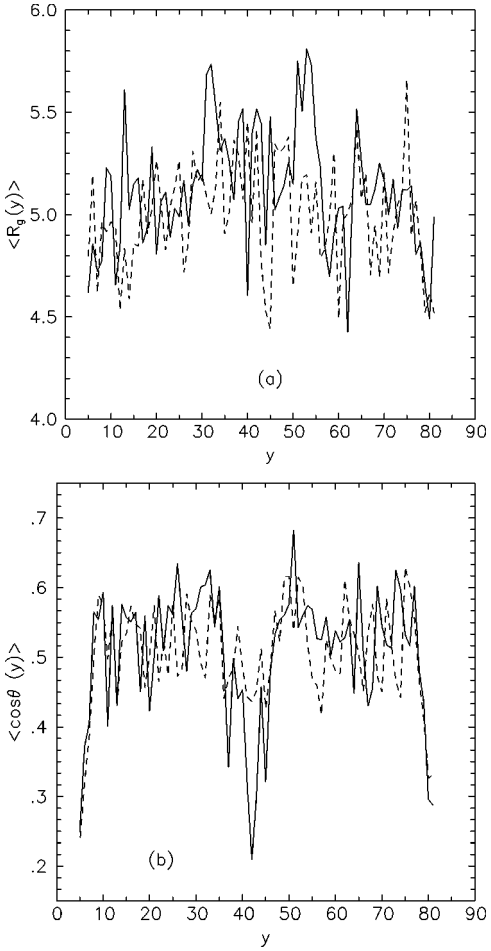

FIG. 16. Molecular relaxation of length-100 chains, in the same format as Fig. 15.

according to position y along the vertical, Figs. 15(a) and 15(b) give the mean radius of gyration and mean cosine of the orientation angle θ for length-10 chains at the same two times as above, again based on 25τ averages. We see that the values are fairly constant within the original bulk regions, both as a function of time and as a function of position, so this system has healed completely within 300τ after merger. (Note that vectors randomly oriented between 0 and 90° have $\langle \cos\theta \rangle = 1/2$, as seen here, and that the angles are likely to be larger at the top and bottom edges of the merged drop, because those molecules will tend to align parallel to the substrates.) The molecular end-to-end separation, an alternative length measurement, is found to have the same trends as the radius of gyration; with a mean value of 3.4. In the case of length-100 chains, Figs. 16(a,b), the results are noisier because there are about ten times fewer molecules in the statistical sample. The radius of gyration has no statistically significant variation, but in the merger region ($y \sim 40-45$) at time 300τ there is a significant dip in the orientation plot: the molecules there have smaller cosines and larger orientation angles with respect to the axis. The latter effect results from molecules partially sticking out of the bulk, whose atoms are relatively free to move parallel to the surface, and whose ends are most likely to be attracted back towards their own drop. The net orientation of such molecules would be somewhat more likely to be horizontal. During coalescence, atoms in such molecules will be attracted to atoms in the other drop at random transverse positions, tending to pin such molecules with a horizontal bias. The orientation persists until somewhat long times, compared for that needed for molecular lengths and atomic densities and displacements to relax to bulk values. The physical mechanism here is that in order for the orientation angles to relax, entire molecules must move with respect to each other. For long entangled chains [23], the relevant mechanism is reptation [24], and rather slow compared to simple atomic diffusion in a liquid.

The standard assumption in applying thermodynamic results to flowing fluid is that the system is in a state of local thermodynamic equilibrium, meaning that the configuration of the molecules in a subregion has an equilibrium probability distribution about the local mean velocity. In the systems considered here, the first test of this assumption is whether the kinetic energy in a subregion has a Boltzmann distribution about the local mean. We observe this behavior (we omit a display of the evidence—see Ref. [25] for a related example). A more stringent test is whether the spatial distribution agrees with that of an equilibrium system, and we observe above that while the pair distribution function and

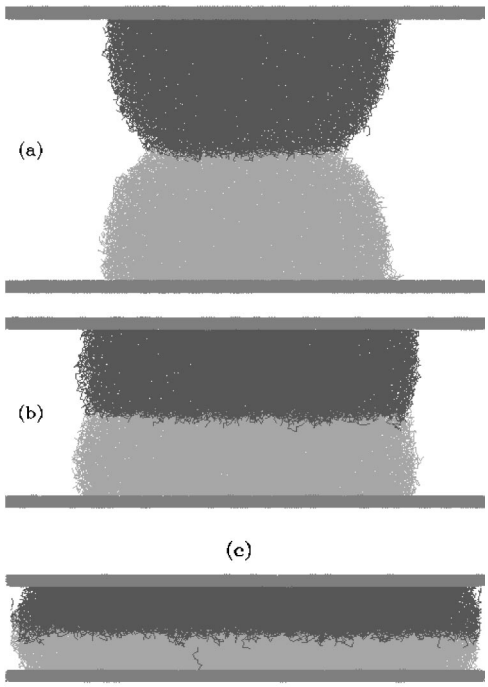

FIG. 17. Snapshots of forced coalescence of length-10 drops as the upper and lower solid plates are moved together at velocities $\pm 0.1\sigma/\tau$: times (a) 50, (b) 150, and (c) 235τ.

various characterizations of molecular shape and orientation show no deviations in the coalescence region, there is a delay in the orientational relaxation. If one were to model the coalescence calculation reported here at the continuum level, the use of equilibrium values for the transport coefficients appears to be almost justified. For the much longer chain lengths of common polymers, the molecular relaxation times are much longer, and there may be a problem. Unfortunately, we do not have the computational resources to address this question quantitatively.

We have also measured continuum flow fields—the velocity and stress tensor. The former just indicates the obvious behavior corresponding to evolution of boundary shape: aside from fluctuations, the only significant flow is confined to the central part of the two-drop system, and simply shows fluid converging towards the merger region. The fluid pressure is largest near the solid substrate, and slightly enhanced in the merger region. The shear stress is small and noisy, with a small signal in the coalescence region resulting from the convergent flow described above. In no case, is there anything resembling a sharp peak, let alone a vestige of singular behavior.

In these simulations, drops have been allowed to coalesce spontaneously, as a result of attractive molecular interactions when the drops are nearby. We now consider forced coalescence, when the two drops are driven together. In Fig. 17, we show a sequence of snapshots of the same system of length-10 chains, when the two solid substrates are moved towards each other at velocities ± 0.1. In physical units, the relative velocity is about 30 m/s. Here, the gap width decreases steadily, forcing the liquid outward. There is again a mixing process occurring in the overlap region, with error function like profiles similar to those shown on Fig. 10; The overall density resembles Fig. 11, an initial dip as the two drops coalesce, which fills in by time 150 to an approximately uniform value—the squeezing is slow enough for the liquid to distort without significant density change. (The mean-square displacements here are not directly comparable, because there is a bulk motion as the drops are squeezed.) The molecular characteristics are affected by the squeezing however: while the molecular lengths show no significant variation with position, and a weak tendency to be elongated by the extensional flow, the molecules are strongly oriented horizontally by this same effect. In this case, there is no distinct behavior in the merger region, since the strong distortion of the entire merged-drop system is the principal effect. Finally, on examining the pair distribution functions at various times in the merger region, the center of the gap, there is some smoothing of $g(r)$—the number and strength of the significant secondary peaks decreases everywhere in the liquid as the merged drop is distorted, indicating a loss of equilibrium structure, which, in contrast, is not seen in free coalescence. We have also considered forced coalescence at a higher speeds, wall velocities $\pm 0.5\sigma/\tau$ as well as the same process with length-100 chains: the qualitative features are similar to the case described above.

VI. CONCLUSIONS

We have shown how MD simulations of nanometer-sized liquid drops may be used to study questions of mass and thermal transport, in the subcontinuum regime where experiments are difficult and theoretical methods uncertain. The procedure used is to generate equilibrated drops of various molecular liquids, which may then be subjected to different forms of external forcing, which correspond to suitable laboratory experiments. From the calculation, one may determine the evolution of both external shapes and bulk motion, as well as the internal structure of the liquid. In addition, one may examine the details of the return to equilibrium after the forcing ceases.

The simulations of cooling of a drop on a substrate produced physically reasonable results, but unfortunately not the dimple formation that was hoped for. We were constrained in these simulations by computational capacity, and were not able to consider Coulombic interactions and the hydrogen bonding of real water, nor examine a complete range of cooling rates. In evaporation, the simulations gave behavior in agreement with a theoretical prediction for partially wetting drops, but we did not explore the parameter range needed to obtain a full understanding of thermal effects in contact line dynamics. Studies of thermal effects on the dynamics of drops of nonpolar liquids are probably possible now, given a bit more patience and computational resources, but the dynamics of water at these length and time scales constitutes more of a challenge.

In coalescence, we have extended earlier studies to consider more realistic molecular systems and different environments for the process. One result is that the microscopic mechanism first observed for a monatomic liquid holds more generally: coalescence begins when a thermal fluctuation al-

lows molecules of one drop to approach those of the second drop closely enough to interact, whereupon these molecules are pulled towards each other and in turn draws out other molecules from its own respective drop into interaction with those of the other drop. At early stages this mechanism produces a tendril of molecules connecting the original drops. In the absence of other constraints, molecules of each drop are steadily pulled into the mutual interaction region, and the joining tendril thickens until the drops merge.

The coalescence process relies on the ordinary attractive interaction between molecules and does not require any unusually close approach or violent molecular motion, so there is no singular behavior in the stress or other fields. There may, however, be relatively rapid motion as the drops rearrange, so some local stress enhancement is possible. In fact, in these simulations there is little or no internal flow outside the coalescence region, and so the only appreciable stress occurs there, but with numerical values that are still only $O(1)$ (in MD units). A second aspect of coalescence studied here was the time scale for healing of the interfacial region. We first observe a relatively rapid relaxation of ''single-atom'' statistics, such as density or mean-square displacement, to equilibrium values. The time scale for density variations is understandable based on the fluid's viscosity, and the behavior of atomic displacements is due to density and geometric considerations. Although it is conceivable that the slow relaxation times associated with polymeric fluids would yield a slower return to equilibrium for measurements of internal correlations and structure, we do not observe such effects. Pair distribution functions and other probability distributions associated with molecular configurations return approximately to bulk values as rapidly as the density does, and there is no significant distinction in this regard between the coalescence and bulk fluid regions. These results support the use of local equilibrium assumptions in applying continuum modeling to nanoscale processes.

ACKNOWLEDGMENTS

We thank S. H. Davis for interesting us in solidification and evaporation, the NASA Microgravity Science and Applications Program for financial support, and the HPCC/ESS project at NASA's NCCS, and NAS Centers, and NPACI at the San Diego Supercomputer Center, for providing computer resources.

[1] M. P. Allen and D. J. Tildesley, *Computer Simulation of Liquids* (Clarendon Press, Oxford, 1987).
[2] C.-M. Ho and Y.-C. Tai, Annu. Rev. Fluid Mech. **30**, 579 (1998).
[3] J. Koplik and J. R. Banavar, Annu. Rev. Fluid Mech. **27**, 257 (1995).
[4] D. M. Anderson, M. Grae Worster, and S. H. Davis, J. Cryst. Growth **163**, 329 (1996).
[5] D. M. Anderson and S. H. Davis, Phys. Fluids **7**, 248 (1995).
[6] S. Schiaffino and A. A. Sonin, Phys. Fluids **9**, 2217 (1997).
[7] J. Koplik and J. R. Banavar, Science **257**, 1664 (1992).
[8] P. Dell'Aversana, J. Koplik, and J. R. Banavar, Phys. Fluids **8**, 15 (1996).
[9] R. B. Bird, C. F. Curtiss, R. C. Armstrong, and O. Hassager, *Dynamics of Polymeric Liquids*, 2nd ed. (Wiley, New York, 1987), two volumes.
[10] B. Busic, J. Koplik, and J. R. Banavar (unpublished); B. Busic, Ph.D. thesis, City University of New York, 2001.
[11] P. A. Thompson and M. O. Robbins, Phys. Rev. Lett. **63**, 766 (1989).
[12] *Monte Carlo and Molecular Dynamics Simulations in Polymer Science*, edited by K. Binder (Oxford, New York, 1995), Chap. Z.
[13] M. Kröger, W. Loose, and S. Hess, J. Rheol. **37**, 1057 (1993).
[14] S. Pal, J. Koplik, and J. R. Banavar (to be published).
[15] M. S. Tomassone, A. Couzis, C. Maldarelli, J. R. Banavar, and J. Koplik, J. Chem. Phys. **115**, 8634 (2001).
[16] J. Koplik and J. R. Banavar, Phys. Rev. Lett. **84**, 4401 (2000).
[17] E. F. Hare and W. A. Zisman, J. Phys. Chem. **59**, 335 (1955); G. Reiter and R. Khanna, Phys. Rev. Lett. **85**, 5599 (2000).
[18] S. Sugano, *Microcluster Physics*, 2nd ed. (Springer, New York, 1998).
[19] J. Koplik and J. R. Banavar, Phys. Fluids A **5**, 521 (1993).
[20] K. Binder, J. Baschnagel, C. Bennemann, and W. Paul, J. Phys.: Condens. Matter **11**, A47 (1999).
[21] J. Eggers, Rev. Mod. Phys. **69**, 865 (1997).
[22] J. Eggers, J. R. Lister, and H. A. Stone, J. Fluid Mech. **401**, 293 (1999).
[23] K. Kremer and G. S. Grest, J. Chem. Phys. **92**, 5057 (1990).
[24] P. G. de Gennes, *Scaling Concepts in Polymer Physics* (Cornell University Press, Ithaca, 1979); M. Doi and S. F. Edwards, *The Theory of Polymer Dynamics* (Clarendon Press, Oxford, 1990).
[25] W. Loose and S. Hess, Phys. Rev. Lett. **58**, 2443 (1987).
[26] J. P. Hansen and I. R. Mc. Donald, *Theory of Simple Liquids* (Academic Press, London, 1976).